Inferring single-cell heterogeneity of bacteriophage life-history traits from population-scale dynamics

Marian Dominguez-Mirazo[1,2,3,+], Ran Tahan[4,+], Shay Kirzner[4], Debbie Lindell[4,o], and Joshua S. Weitz[3,5,6,o]

[1]School of Biological Sciences, Georgia Institute of Technology, Atlanta, GA, USA
[2]Interdisciplinary Graduate Program in Quantitative Biosciences, Georgia Institute of Technology, Atlanta, Georgia, USA
[3]Department of Biology, University of Maryland, College Park, Maryland, USA
[4]Faculty of Biology, Technion – Israel Institute of Technology, Haifa, Israel
[5]Department of Physics, University of Maryland, College Park, Maryland, USA
[6]University of Maryland Institute for Health Computing, North Bethesda, Maryland, USA
[+]These authors contributed equally to this work
[o]Corresponding authors: JSW (jsweitz@umd.edu) and DL (dlindell@technion.ac.il)

March 25, 2025

Abstract

Phage-induced lysis of bacteria transforms population dynamics, community structure, and ecosystem functioning. Scaling up infected cell fate to ecosystem-scale impacts requires quantitative estimates of viral life history traits, including underlying heterogeneity in the timing, efficiency, and outcome of lytic infections. Here, we apply a nonlinear model of phage-bacteria infection dynamics to infer single-cell heterogeneity of phage-induced lysis from population-scale time series. We evaluate this inference approach in an ecologically relevant system: Syn9, a T4-like cyanophage infecting *Synechococcus* strain WH8109, a representative of globally abundant marine cyanobacteria. The model infers heterogeneous distributions of latent period and burst size that were subsequently validated using a single-cell assay. We find observed latent period variation exceeds that found in coliphage with holin lysis systems and that burst size variability is largely explained due to latent period variation. These findings demonstrate the feasibility of inferring phage trait heterogeneity from population data in ecologically relevant systems even in the absence of single-cell experiments.

1 Introduction

Bacteriophage (phage) adsorb, infect, and lyse sensitive bacteria, transforming the fate of cells and populations. Cumulatively, phage are estimated to kill a substantial fraction of marine microbes daily in surface waters [1] (with estimates spanning 1-5% in oligotrophic gyres [2, 3] to ∼10-30% in transition zones [3, 4]), and potentially higher levels during blooms [5–7]. The lysis of marine microbes leads to the release of organic matter back into the microbial loop [7–10] and may generate sticky aggregates that can lead to increases in export of organic matter in the water column [6, 11, 12].

The viral lytic life cycle includes multiple stages: phage adsorb to bacterial cell surfaces, inject their genetic material into the cytoplasm, hijack cell machinery to produce new infectious virions, and finally lyse the host cell, releasing viral progeny back into the environment. The different stages are represented in terms of 'viral life history traits', including the adsorption rate, latent period (time between attachment and lysis) and the burst size. Conventionally, these viral life history traits are quantified via a single number that may differ between phage-bacteria pairs [13, 14] and can be modulated by environmental conditions (e.g., temperature [13, 15]) or nutrient availability (e.g., nitrogen and phosphorus [16, 17]).

In fact, phage life history traits can exhibit considerable variability even within a phage-host pair given fixed environmental conditions [18–20]. The intrinsic variability of life-history traits influences microbial population dynamics because of compounding effects of heterogeneity. For example, viruses released during relatively early lysis events within a population of infected cells can go on to infect new cells earlier than those viruses that lyse relatively later on [21–24]. Previous work has attempted to circumvent these technical challenges and characterize life-history trait variability, in particular that of the latent period, from population-level data [21]. Although latent period variability has been characterized within some host-phage systems, these studies typically focus on *E. coli*-infecting phage where the latent period

is tightly regulated with a coefficient of variation that ranges between 0.05 and 0.17 [24–27]. Whether or not such variability is common or conserved across diverse phage-host systems remains unresolved.

In this study, we apply a nonlinear mathematical modeling framework to infer bacteriophage latent period distributions from population-scale time series and develop a single-cell lysis assay to test model-inferred predictions. We do so by focusing on Syn9, a lytic T4-like cyanophage infecting *Synechococcus* sp. WH8109, a representative of globally abundant cyanobacteria. Cyanobacteria are the most abundant photosynthetic organisms on the planet [28, 29]. Cyanophages play a significant role in shaping the ecology and evolution of cyanobacteria [30–32] and, in turn, influence the global flow of carbon and nutrients [1, 9]. By fitting data to a lytic infection model that accounts for latent period variability, we demonstrate that population-level data can be used to accurately predict latent period variability as validated using single-cell assays. Furthermore, we show that intrinsic variability in the latent period also explains variation in Syn9 burst size. Together, this study jointly characterizes latent period and burst size variability in an ecologically relevant system via population-level and single-cell data, while offering a framework for similar investigations in other systems even when single-cell data is unavailable.

2 Results

2.1 Lysis time distributions recapitulated from population-level time series

Standard methods for estimating bacteriophage life-history traits, i.e. one-step growth curves, rely on measuring the accumulation of free virus during a single round of infection. The latent period is typically reported as a single value, generally approximated by the time of the first visible burst or, less commonly, the midpoint of the rise [14, 33]. However, in the presence of intrinsic variability in the latent period, this single-value estimate introduces biases in trait characterization and does not capture potential variability at the single-cell level [21]. Additionally, one-step growth curves fail to provide enough information to recapitulate latent period distributions (described in terms of mean and variance), while time series of multiple rounds of infection – multi-cycle response curves – potentially allow for the accurate prediction of underlying trait distributions [21].

Here, we characterize the latent period distribution of the Syn9 phage during infection of the marine cyanobacterium *Synechococcus* sp. WH8109. A 'multi-cycle response curve' was obtained by inoculating phage in a population of *Synechococcus* growing in liquid culture. Plaque assays were used to quantify the number of infective viruses at multiple time points from 0 to 24 hours after inoculation, capturing multiple cycles of infection (Figure 1A). We used a nonlinear, differential equation model to describe the interactions between lytic phage and bacteria (Figure 1B) [21]. The model presents a microbial population in which the timing of infected cell lysis follows an Erlang distribution, a continuous probability distribution that results from the sum of exponentially distributed events (Figure S1). This distribution can be defined with the mean and coefficient of variation (CV) of the latent period (see Materials and Methods). We used a previously described Bayesian inference framework to fit the model to the 'multi-cycle response curve' [21], finding the life-history trait values, including the latent period distribution, that allow the mechanistic model to best describe the data (Figure 1C) (see Table S1 for all parameter estimations, and Figure S2 for chain convergence analysis). A single-value estimate based on the time of the appearance of the first burst would define the latent period to range between 4 and 4.5 hr (Figure 1C). In contrast, the Bayesian inference predicts a latent period mean of 7 hr with a 95% Confidence Interval (CI) ranging from 6.7 to 7.5 hr with a predicted CV of 0.15 with CI 0.13 to 0.18 (Figure 1D).

2.2 Single-cell heterogeneity in lysis time

We set out to test our population-level predictions using single-cell data. Note that single-cell data from this host-virus system was not used to develop the population-level framework nor used as part of population-level inference. We devised a protocol for single-cell lysis detection adapted from previous work intended to determine the variability of virus progeny production [20]. Briefly, we infected a *Synechococcus* population growing in liquid media with phage Syn9 at a relatively high host density and phage-host ratio to maximize contacts. After 15 minutes, the population was diluted to reduce phage-bacteria encounters and ensure that all infections resulted from encounters that occurred within this time window. Individual cells were isolated, placed into single wells, and incubated in growth conditions. The contents of 30 wells were plated using the plaque assay every half hour, to quantify cell lysis and virus production, starting at 4 hrs and ending at 12 hrs after initial infection (Figure 2A - full details available in the Materials and Methods).

By the time of sampling, three scenarios could have occurred within the individual well (Figure 2B): (i) The cell in the well was not infected. Under this scenario, the plaque assay would result in no visible plaques. (ii) The cell was infected but did not lyse before the well contents were plated. Here, cell lysis

would occur on the plate and all virions would be released from the same location, resulting in a single plaque. (iii) The cell lysed before the well contents were sampled. At the time of sampling the contents of the well were primarily free virions. When the contents were used for plaque assays, each individual virion would be plated in a different spot, resulting in as many plaques as infective viral particles - a proxy for that individual cell's burst size. If the infected cell released a single infective particle, there would be a single plaque. Note that cells that were infected but not lysed by the sampling time point and cells lysed with a burst size of one infective particle would both result in a plaque count of 1. These two scenarios are indistinguishable from each other [20] (Figure 2B).

If we assume that no infections (or a negligible number) result in a burst size of 1, we can approximate the number of cells lysed by the sample time point as the number of plates with 2 or more plaques (scenario iii). We can calculate the total number of successful infections by counting the plates that have 1 or more plaques (adding scenarios ii and iii). Then, the probability that a cell had lysed by the sample time point is the ratio between the number of lysed cells (scenario iii) and the total number of infections (the sum of scenarios ii and iii). Following the increase of probability across time gives us the Cumulative Distribution Function (CDF) of the lysis time distribution (Figure 2C). At time 4 hr after initial infection, we start observing plaque assays with 2 plaques or more. The proportion of lysed to infected cells plateaus at about 10 hrs after initial exposure. Interestingly, even after 12 hrs, the proportion of lysed to infected cells does not reach 1, i.e. not all infected cells have been lysed and/or some infections result in a burst size as small as 1 viral particle per infected cell (or equivalently, one plaque-forming unit) (Figure 2C).

By considering burst sizes of 1 (see Materials and Methods, Figure S3), we find that the single-cell latent period data is best described by a Gamma distribution with mean 7.4 hr (CI: [6.8, 8.3]) and CV 0.23 (CI: [0.17, 0.33]) (Figure 2C,D). This estimation of latent period heterogeneity is larger than that observed in other phage-bacteria with holin lysis systems [24–26], an issue we address in the discussion. The latent period distribution predicted using population-level time series is described by an average and CV that fall within the confidence intervals obtained from the single-cell data (Figure 2D). Similarly, the average burst size is successfully predicted by the population-level method (Figure S4). These results show that single-cell scale heterogeneity of viral life history traits can be recapitulated from population-level dynamics (see Figure S5-7 for evidence on our ability to infer latent period distributions using data from the 'single-cell lysis detection protocol').

2.3 Lysis time variability influences burst size

In addition to providing information on the latent period distribution, the single-cell experiment provides information on the effective burst size of the cumulative latent period, i.e. the average burst size of individual cells that lysed by the sampling time point t. If there is a relationship between latent period and burst size, the average burst size at each experimental time point would be the weighted sum of the latent period to burst size function, where the weights reflect the lysis probability in the latent period distribution normalized to time t (see Methods). If the burst size increases with the latent period, the effective burst size over the cumulative lysis time will also increase. Indeed, we observe that the effective burst size increases with sampling time (Figure 3A). The effective burst size begins to plateau around 10 hours after infection, which coincides with a latent period after which few new lysis events occur (Figure 2D).

We analyze three models describing the relationship between latent period and burst size: (i) a piecewise linear model, (ii) a saturating model represented by a Hill function, and (iii) a logistic growth model that characterizes the lysis time–burst size relationship in chemically induced lysis of individual λ lysogens [34]. We find that a piecewise linear model for a latent period to burst size function that incorporates the latent period distribution (Figure 2D) and corrects for time-dependent adhesion of virions to the well surface in our experimental protocol (Figure S8, Materials and Methods), minimizes the mean squared error for the effective burst size of the cumulative latent period across four replicates (Figure 3A). The model predicts a time of initial burst at 4.8 hr after infection [CI: 3.7, 5.2], and a rate of progeny production of 27.4 infective viral particles per hour [CI: 15.0, 34.9]. To validate this model, we infer which specific lysis events occurred at time intervals of half an hour, given the burst size distributions at different sampling times (see Materials and Methods). Our predictions support a linear latent period to burst size model after a delay to first burst (Figure 3B, Figure S9). Note that this linear relationship may only hold in the lysis time interval between 5 to 10 hrs, after which the probability of new lysis events drops significantly. As observed by Kannoly *et al.* [34], long lysis times would result in the depletion of bacterial resources and a latent period to burst size function that flattens at longer times. Our results suggest that heterogeneity in progeny production is a direct result of variability in lysis time (Figure 3C).

3 Discussion

In this study, we characterized the latent period distribution of the cyanophage Syn9 when infecting *Synechococcus* sp. WH8109 using two complementary approaches. First, we applied a population-level framework from 'multi-cycle response curves' to infer life-history traits, leveraging viral density time series data [21]. Second, we developed a single-cell lysis detection protocol, building on previous work examining variability in viral progeny production [20]. The single-cell method confirms that lysis time heterogeneity at the single-cell level can be captured by population-level data. In addition, this protocol allowed us to explore the relationship between burst size and latent period at the single-cell level. We find that burst variability is shaped by intrinsic lysis time variability with burst sizes continuing to rise linearly as a function of the latent period – and not saturating within relevant regimes.

Inherent heterogeneity is a well-established phenomenon observed across a wide range of viral systems [35–38]. However, studying variability in microbial systems comes with the intrinsic challenges of performing single-cell measurements. These limitations have led to the development of population-level methods for characterization of viral life-history traits, i.e. the one-step growth curve, that often obscure the presence and impact of heterogeneity in microbial dynamics [21]. Here, we extended a recently proposed method [21] to predict life-history traits from population-level time series using single-cell information, with a focus on joint estimates of latent period and burst size variation. We showed that it is possible to reliably estimate latent period distributions at single-cell scales from population-level data. Doing so also removes biases in conventional estimates of the latent period mean while making it possible to extend the method to diverse phage-host systems.

We estimated the Coefficient of Variation (CV) of the latent period distribution for Syn9 to be 0.23. In comparison, measurements of lysis time variability in induced λ lysogens report CV levels ranging between 0.05 to 0.12 for various mutants [25, 26]. Similarly, the CV for phage T7 is estimated to be 0.15 [24]. A CV of 0.23 for Syn9 suggests that lysis will most likely occur between 4 and 11 hours. Although this variability is larger than previously observed for other coliphage systems including λ, T7, and T4, the observed variability in lysis time remains low compared to other viral processes and traits, such as burst size, DNA injection time, or lysogenization decisions [19, 24, 39]. The molecular mechanisms governing latent period have typically been characterized in dsDNA phage with holin-dependent lysis systems infecting gram-negative bacteria like *E. coli* [40, 41]. In those systems, holins act as a clock potentially tightly regulating lysis timing [42–45]. In contrast, single-gene lysis systems often exhibit greater variability in lysis timing with CV values up to 0.48 [27, 41]. Further work would help elucidate whether a holin-based mechanism helps explain the relative levels of lysis time variability for Syn9 despite the much longer average latent period relative to that of coliphage-bacteria systems.

In this study we were able to infer both latent period and burst size variation at single-cell scales. The variability in burst size has been recognized since foundational studies of phage biology [18–20], however the origins of burst size variability have remained elusive. Burst size variation is likely influenced by factors such as cell physiology, size, and virus-host compatibility [18, 24, 46–48]. A positive and linear nature of the latent period to burst size relationship has been previously suggested [49] and is commonly incorporated in the study of life-history trait evolution [50–55]. This relationship has primarily been observed at the population level. In this study, we provide the first single-cell resolution evidence that burst sizes increase linearly without saturation under physiologically relevant regimes. In contrast, a recent single-cell study suggested that the rate of progeny production may initially be exponential, followed by a plateau as cellular resources are depleted [34]. In the referenced study, cells were artifically lysed, enabling longer latent periods than those expected from intrinsic lysis time variability alone, which in turn allowed for the emergence of a plateau. Our results raise questions about the role of variability in viral fitness and evolution. Further research is needed to explore whether and how latent period variability stems from a trade-off between burst size and lysis time, either as an unavoidable consequence of molecular stochasticity or as a bet-hedging strategy for adapting to fluctuating environments [24, 26, 56].

This study comes with caveats, both specific to our choice of ecologically relevant virus-host pair and the relevance of our findings to other systems. For example, cyanobacteria are particularly sensitive to changes in light availability, including levels and duration over day-night cycles, which impact viral adsorption and production [57–59]. Additionally, resource availability and interactions with other bacterial species and phages may further impact traits (e.g., due to changes in the availability of nitrogen and phosphorus [16, 17]). The inclusion of resource limitation and additional environmental complexity may lead to even greater variability than that observed in laboratory settings. We anticipate that incorporating other forms of ecological feedback into the 'multi-cycle response curve' inference framework will enable estimates of single-cell latent period variability under a wider range of ecologically relevant conditions. Given the generality of the framework, we are optimistic that the underlying mathematical model and single-cell assay can be adapted to other phage-bacteria systems, either separately or in combination.

In closing, we have shown that it is possible to accurately infer heterogeneity in lysis-associated life history traits at single-cell scales from population-scale dynamics. Notably, the single-cell assay measurements of latent period variability are within the confidence intervals predicted by our population-scale inference framework. Moreover, we have determined that variation in the latent period is a major contributor to realized variation in burst size. We anticipate that quantifying the variability of life-history traits in phages will help identify mechanistic principles underlying lysis timing variation and enable the development of predictive models of viral impacts in therapeutic and environmental contexts.

4 Materials and Methods

4.1 Bacterial culture growth and phage propagation

Synechococcus WH8109 cultures were grown in artificial sea water (ASW) medium [60] with modifications as described in Lindell *et al.* [61], at 21°C and a light intensity of 45 μmol photons $m^{-2}s^{-1}$ under a 14:10 light-dark cycle with gentle shaking. Cell density was enumerated using the Influx flow cytometer (BD Biosciences). Cultures of *Synechococcus* were excited with a 457-nm and 488-nm laser and detection based on their orange fluorescence (emission at 580/30 nm) and forward scatter. Yellow-green 1-μm-diameter microspheres (Fluoresbrite) were added to each sample as an internal standard for size and fluorescence. Cell density and culture growth prior to experiments was approximated using chlorophyll *a* fluorescence (excitation at 440 nm, emission at 660 nm) measured in 96-well plates using a Synergy Mx Microplate Reader (Biotek).

Phages were propagated by infecting *Synechococcus* WH8109 cultures at a multiplicity of infection (MOI) of ∼0.1. After 24 hours, the lysate was centrifuged at 5467 g for 5 minutes to remove residual host cells and filtered through a 0.22 μm syringe filter (Millex-GV, Millipore) to remove cell debris. The concentration of infective phages was enumerated using the plaque assay. Lysates were diluted and pour-plated in plates containing *Synechococcus* WH8109 at sufficient concentrations to produce lawns. Pour-plating was performed as previously described [62] using ASW medium supplemented with 1 mM sodium sulfite [63] and 0.28% low melting point agarose (Invitrogen) [63, 64].

4.2 Virus multi-cycle response curve

Multi-cycle virus-host infection dynamics assays were performed by infecting *Synechococcus* WH8109 cultures ($\sim 5 \times 10^7$ cells/mL) at a MOI of ∼0.1. Samples of 0.1 mL from the infected culture were collected, diluted with 0.9 mL of medium, and filtered through a 0.22 μm syringe filter (Millex-GV, Millipore) to remove host cells. The number of infective phages in the filtrate was then determined by the plaque assay. Four independent biological replicates were performed at different times.

4.3 Single-cell lysis detection protocol

To recapitulate the latent period distribution of Syn9 infecting *Synechococcus* WH8109 we conducted a single cell infection experiment. *Synechococcus* WH8109 (1.2×10^8 cells/mL) was infected at an MOI of 2 and diluted 3000-fold after 15 minutes. This was done to limit adsorption time and thus infections, allowing us to measure the latent period at a 15-minute time resolution, and to prevent co-sorting of free phages and cells as previously described [20]. Single cells were then sorted into 96-well plates containing medium using an Influx flow cytometer. To reduce oxidative stress for the sorted cells a heterotrophic helper *Alteromonas* sp. EZ55, was added to the medium in the wells as previously described [20, 65]. The number of infective phages produced by 30 single cells was determined every 30 minutes from 4 to 12 hours post infection by plaque assay. This was done by plating the entire content of a single well on a plate, as previously described [20]. Four independent biological replicates were performed at different times.

To estimate the adsorption of infective phages to plastic during the experiment we tested changes in titer of a Syn9 lysate in a 96-well plate over an 8 hour period. The Syn9 lysate was diluted with ASW containing helper bacteria to 90 plaque forming units per milliliter. The diluted lysate was aliquoted in 96-well plates and the entire contents of 6 of the wells was assayed periodically by plaque assay. We also measured the number of infective phages prior to putting the lysate in the 96-well plate to quantify the loss of phages from small amounts of liquid loss in the wells.

4.4 Predicting life-history traits from population-level time series

We use a modified version of a lysis model accounting for lysis time variability from Dominguez-Mirazo *et al.* [21], described here for clarity. The system of nonlinear differential equations includes susceptible

cells, S, free viruses, V, exposed cells, E, and actively-infected cells, I. Susceptible cells, S, have a maximal cellular growth rate μ (hr^{-1}) and a total cell population carrying capacity K(cells/ml) where $N = S + \sum_{k=1}^{n} E_k + I$ gives the total cell population. We assume that infected cells at any stage of infection do not grow and that cell death rates and viral decay rates are negligible compared to other key rate constants of the system. We assume that viruses and hosts are well-mixed. The rate at which susceptible cells (S) are infected is given by: $i(t) = \phi\, S\, V$, where ϕ(ml/hr) denotes the adsorption rate. Infected cells at any stage can adsorb phage at the same rate as susceptible cells without consequences to the ongoing lytic cycle.

We incorporate variability in latent period by assuming that before entering the actively-infected stage, I, infected cells advance through several exposed E stages: $E_1, \ldots, E_n$, where n is a non-negative integer. There are $n+1$ transitions, and exposed cells (E) transition between compartments at a rate of $(n+1)\,\eta$ with exponentially distributed times. The average time from adsorption (*i.e.*, entering the first Exposed class, E_1) to cell burst (*i.e.*, exiting the actively-infected class, I) is the latent period mean and equals the inverse of the mean lysis rate, $T = 1/\eta$. At the end of the actively-infected stage (I), the cell bursts and free virus (V) increases from viral release of β virions. The system of nonlinear, ordinary differential equations can be written in the form:

$$
\begin{aligned}
\dot{S} &= \overbrace{\mu\, S \left(1 - \frac{N}{K}\right)}^{growth} - \overbrace{\phi\, S\, V}^{adsorption} \\
\dot{E}_1 &= \overbrace{\phi\, S\, V}^{adsorption} - \overbrace{(n+1)\,\eta\, E_1}^{transition} \\
\dot{E}_2 &= (n+1)\,\eta\,(E_1 - E_2) \\
&\vdots \\
\dot{E}_n &= (n+1)\,\eta\,(E_{n-1} - E_n) \\
\dot{I} &= (n+1)\,\eta\,(E_n - I) \\
\dot{V} &= \overbrace{\beta\,(n+1)\,\eta\, I}^{burst} - \overbrace{\phi\,(S + \sum_{i=1}^{n} E_i + I)\, V}^{adsorption}
\end{aligned}
\tag{1}
$$

This model describes the latent period distribution as an Erlang distribution with shape $n+1$ – the number of exposed (E) compartments plus the infected (I) compartment –, and rate η – the lysis rate. In this form, the mean (T), variance (σ^2), and coefficient of variation (σ/T) of the latent period (LP) are given by:

$$\text{Mean(LP)}: \quad T = \frac{1}{\eta} \tag{2}$$

$$\text{Var(LP)}: \quad \sigma^2 = \frac{T^2}{n+1} \tag{3}$$

$$\text{CV(LP)}: \quad \frac{\sigma}{T} = \frac{1}{\sqrt{n+1}}\ . \tag{4}$$

Therefore, the number of E compartments dictates the spread of the distribution through the coefficient of variation (CV), with larger n leading to tighter distributions and smaller CV values (Figure S1). Since n must be an integer, this imposes constraints on the CV values that can be simulated. For example, $n = 0$ corresponds to a CV of 1, and $n = 1$ results in a CV of approximately 0.7. As a result, the model cannot represent CV values between 0.7 and 1. However, latent period distributions with CV below 0.5 can be accurately simulated with a tolerance of 0.05. Based on estimates of lysis timing variability from various studies [24, 25, 27], we anticipate that CV values for latent periods in natural systems will be less than 0.5, aligning with the model's ability to capture variability in latent period timing.

We leverage a computational pipeline previously designed to fit model parameters to data [21] (see Table S1 for parameter estimates). Briefly, we implement a Markov Chain Monte Carlo (MCMC) algorithm using the Turing package in Julia [66] and inform prior distributions using biological knowledge of the phage bacteria system (see Table S2). We obtain 95% confidence intervals by sampling the MCMC posterior distributions. Convergence analysis can be found in Figure S2.

4.5 Predicting latent period distributions from single-cell data

Under our experimental setup, plaque assays at each time point can yield one of three possible outcomes:

1. **No plaques visible:** This outcome indicates the isolated cell was not successfully infected, either because it did not encounter a phage during the co-incubation period or because the infection failed. Previous studies have shown that not all phage-bacteria encounters result in successful infections [20].

2. **One plaque is visible:** A single plaque can result from two types of events: 1) the cell was infected but had not yet lysed by the time the sample was plated. In this case, the infected cell is added to the plate and continues intracellular viral production. When the cell bursts, all virions will be released at a single location in the plate, which results in the formation of a single plaque. 2) The cell was successfully infected and had lysed a single virion (burst size of 1) prior to plating. These two scenarios are indistinguishable under our protocol.

3. **Multiple plaques are visible:** This outcome indicates that cells have lysed and released virions at some point prior to plating. The plaque number represents the burst size of the individual lysed cell.

If we assume the burst size is always larger than 1, the number of plates with multiple plaques reflects the number of infected cells that had lysed by time t (denoted as $k(t)$), where t is the sampling time point. The total number of successful infections observed at each time point ($n(t)$) is the sum of scenarios 2 (infected but unlysed cells at the time of plating) and 3 (lysed cells). The proportion of successful infections that had lysed by time t ($k(t)/n(t)$) represents the cumulative distribution function of the lysis time distribution. If we were to sample at an infinite time point, we would expect all infected cells to have lysed, resulting in a proportion of 1.

We consider two probability distributions with non-negative support: the log-normal and the gamma distribution. Both distributions can be described in terms of the mean lysis time (T) and the coefficient of variation (CV), as

$$\tau \sim LogNormal(\mu, \sigma)$$
$$\mu = ln(T) - \frac{1}{2} ln(1 + CV^2)$$
$$\sigma = \sqrt{ln(1 + CV^2)}$$

and

$$\tau \sim Gamma(\alpha, \theta)$$
$$Shape(\alpha) : \alpha = \frac{1}{CV^2}$$
$$Scale(\theta) : \theta = T\,CV^2$$

For a combination of latent period mean and CV, we calculate the probability of an infected cell having lysed by the sampling time $p(t)$, based on the cumulative distribution function (CDF) of either the gamma or log-normal distribution. The probability of observing our data at each sampling point follows a binomial distribution:

$$P(X = k) = \binom{n}{k} p^k (1 - p)^{n-k}$$

where k represents the number of observed lysed cells at the sampling time point, out of n infected cells, and p is the lysis probability derived from the corresponding latent period CDF.

To account for infections that result in a burst size of 1, we add a parameter y where $1 - y$ is the proportion of infected cells we expect to have a burst size of 1. The probability of observing our data at each sampling point follows:

$$P(X = k) = \binom{n}{k} (yp)^k (1 - yp)^{n-k}$$

The Maximum Likelihood Estimate (MLE) corresponds to the model (defined by the distribution type (gamma or log-normal), y, mean latent period (T), and CV) that maximizes the likelihood of observing our data (Figure S3, Table S3). We search for the MLE using the fminsearch MATLAB(R2024a) function, starting the search at multiple combinations of random initial parameters. To calculate parameter

confidence intervals, we used profile likelihood methods. In this approach, one parameter is fixed while the confidence interval for the non-fixed parameter is computed. The likelihood ratio is then compared to a chi-square distribution at a significance level of 0.05. With this experimental protocol and prediction framework, we are able to accurately characterize the latent period distributions for a range of relevant values (Figure S6-7).

4.6 Burst size as a function of lysis time

For those plaque assays where the number of plaques is larger than 1, the plaque count reflects the burst size of individual cells. At each sample time point t, the plaque count of these assays reflects the observed burst size of cells that lysed by time t. The effective burst size at each sampling point that we expect to observe in our protocol is given by,

$$\overline{\beta_t} = \frac{\int_0^t e^{-0.04(t-\tau)}\,\theta(\tau)\,P(\tau)\,d\tau}{\int_0^t P(\tau)\,d\tau}$$

where $P(\tau)$ is the latent period distribution, $\theta(\tau)$ is the burst size as a function of the latent period, and the exponential part accounts for time-dependent viral particle adhesion to the well's surface in our experimental protocol (Figure S8). This equation can be thought of as a sum of expected burst sizes at lysis times shorter than t, corrected for particle adhesion, and weighted by the normalized probability of the lysis times.

Leveraging our latent period distribution $P(\tau)$, we evaluate multiple models of expected burst size $\theta(\tau)$.

1. Linear model

$$\theta(\tau) = \begin{cases} r\,(\tau - d), & \text{if } \tau > d \\ 0, & \text{otherwise} \end{cases} \tag{5}$$

   where r is the progeny production rate and d is the time at which the first cell lyses.

2. Hill function

$$\theta(\tau) = \begin{cases} k_{max}\,\frac{\tau - d}{(\tau_{50} - d) + (\tau - d)}, & \text{if } \tau > d \\ 0, & \text{otherwise} \end{cases} \tag{6}$$

   where d is the time at which the first cell lyses, k_{max} is the maximum burst size, and τ_{50} is the time at which the expected burst size reaches half of k_{max}.

3. Logistic growth model sourced from [34].

$$\theta(\tau) = \begin{cases} k_{max}\,\frac{e^{r(\tau-d)}-1}{e^{r(\tau_{50}-d)}+e^{r(\tau-d)}-2} & \text{if } \tau > d \\ 0, & \text{otherwise} \end{cases} \tag{7}$$

   where d is the time at which the first cell lyses, k_{max} is the maximum burst size, and τ_{50} is the time at which the expected burst size reaches half of k_{max}.

We find the model that minimizes the Root Squared Mean Error (RSME) using the fminsearch MATLAB(R2024a) function, starting the search at multiple combinations of random initial parameters (Figure S9). We calculate confidence intervals for parameters by bootstraping the data and repeating the search for best parameter combinations, defining a 95% CI as those parameter values that fall within quantiles 0.025 and 0.975.

4.6.1 Inferring lysis events at short time intervals

We use Gaussian Mixture Models to infer the lysis events that occurred in half-hour time intervals. We assume that the probability distribution of burst sizes observed at sample time point t_2 (P_{t_2}) can be described as the collection of burst sizes drawn from two distributions: the burst size distribution of lysis events occurred by sample point t_1 (P_{t_1}), and the burst size distribution of lysis events occurred in the half-hour interval between time points t_1 and t_2 (Q) such that

$$P_{t_2} = \frac{P_{t_1}\, w_1 \,+\, Q\, w_Q}{w_1 \,+\, w_Q}$$

where the weights (w) express the probability of lysis events occurring between time 0 and t_1 (w_1), and t_1 and t_2 (w_Q) normalized by the probability of lysis events occurring between 0 and t_2 given a latent period distribution P(τ),

$$w_2 = \int_0^{t_2} P(\tau)\, d\tau$$

$$w_1 = \frac{\int_0^{t_1} P(\tau)\, d\tau}{w_2}$$

$$w_Q = \frac{w_2 \,-\, w_1}{w_2}$$

We fit a Gaussian Mixture Model with two components (P_1 and Q). For the first component, we assume a mean and standard deviation equal to the observed burst sizes at time point t_1. For the second component, we initialize the mean and standard deviation estimates to the moments at time point t_2. The initial assumption for the first component and the fit for the second component are used to cluster the burst sizes observed at t_2. The burst sizes that clustered into the second component are lysis events predicted to have occurred in the half-hour interval between t_1 and t_2.

4.7 Code and data availability statement

We implement the population-level model (Equation 1) and MCMC fitting in Julia v1.7.2 [67] adapted from Dominguez-Mirazo *et al.* [21]. All other analyses were performed in Matlab R2024a [68]. Experimental data and code for simulations and graphics is available at:
https://github.com/WeitzGroup/InferringSingleCellHetereogeneity.git
and archived at:
https://doi.org/10.5281/zenodo.15060329

5 Author contributions

MDM, RT, DL and JSW conceived the study. MDM, RT and SK designed the experiments with input from DL and JSW. RT performed experiments with guidance from SK and DL. MDM performed data analysis with guidance from JSW. MDM drafted the manuscript with contributions from all authors.

6 Acknowledgments

This research was supported by grants from the Simons Foundation Life Sciences Program 735081 and 529554 to DL and 722153 to JSW. Funding sources had no role or influence on study design, analysis, interpretation, or submission. We thank Tapan Goel for code review. We thank Hagit Tahan for contributions in creating the illustrations. This research was supported in part through research cyber infrastructure resources and services provided by the Partnership for an Advanced Computing Environment (PACE) at the Georgia Institute of Technology, Atlanta, Georgia, USA.

References

1. Suttle, C. A. Marine viruses—major players in the global ecosystem. *Nature Reviews Microbiology* **5,** 801–812 (2007).
2. Beckett, S. J., Demory, D., Coenen, A. R., Casey, J. R., Dugenne, M., Follett, C. L., Connell, P., Carlson, M. C., Hu, S. K., Wilson, S. T., *et al.* Disentangling top-down drivers of mortality underlying diel population dynamics of *Prochlorococcus* in the North Pacific subtropical gyre. *Nature Communications* **15,** 2105 (2024).
3. Carlson, M. C., Ribalet, F., Maidanik, I., Durham, B. P., Hulata, Y., Ferrón, S., Weissenbach, J., Shamir, N., Goldin, S., Baran, N., *et al.* Viruses affect picocyanobacterial abundance and biogeography in the North Pacific Ocean. *Nature Microbiology* **7,** 570–580 (2022).
4. Shopen Gochev, C., Demory, D., Lopes dos Santos, A., Carlson, M. C., Gutiérrez-Rodríguez, A., Weitz, J. S. & Lindell, D. Cold surface waters of the sub-Antarctic Pacific Ocean support high cyanophage abundances and infection levels. *Environmental Microbiology* **27,** e70031 (2025).

5. Baudoux, A.-C., Noordeloos, A. A., Veldhuis, M. J. & Brussaard, C. P. Virally induced mortality of Phaeocystis globosa during two spring blooms in temperate coastal waters. *Aquatic Microbial Ecology* **44,** 207–217 (2006).

6. Guidi, L., Chaffron, S., Bittner, L., Eveillard, D., Larhlimi, A., Roux, S., Darzi, Y., Audic, S., Berline, L., Brum, J. R., *et al.* Plankton networks driving carbon export in the oligotrophic ocean. *Nature* **532,** 465–470 (2016).

7. Vincent, F. & Vardi, A. Viral infection in the ocean—a journey across scales. *PLoS Biology* **21,** e3001966 (2023).

8. Wilhelm, S. W. & Suttle, C. A. Viruses and nutrient cycles in the sea: viruses play critical roles in the structure and function of aquatic food webs. *Bioscience* **49,** 781–788 (1999).

9. Breitbart, M., Bonnain, C., Malki, K. & Sawaya, N. A. Phage puppet masters of the marine microbial realm. *Nature Microbiology* **3,** 754–766 (2018).

10. Weitz, J. S. & Wilhelm, S. W. Ocean viruses and their effects on microbial communities and biogeochemical cycles. *F1000 Biology Reports* **4** (2012).

11. Weinbauer, M. G. Ecology of prokaryotic viruses. *FEMS Microbiology Reviews* **28,** 127–181 (2004).

12. Sullivan, M. B., Weitz, J. S. & Wilhelm, S. Viral ecology comes of age. *Environmental Microbiology Reports* **9,** 33–35 (2017).

13. De Paepe, M. & Taddei, F. Viruses' life history: towards a mechanistic basis of a trade-off between survival and reproduction among phages. *PLoS Biology* **4,** e193 (2006).

14. Jin, T. & Yin, J. Patterns of virus growth across the diversity of life. *Integrative Biology* **13,** 44–59 (2021).

15. Demory, D., Weitz, J. S., Baudoux, A.-C., Touzeau, S., Simon, N., Rabouille, S., Sciandra, A. & Bernard, O. A thermal trade-off between viral production and degradation drives virus-phytoplankton population dynamics. *Ecology Letters* **24,** 1133–1144 (2021).

16. Clasen, J. L. & Elser, J. J. The effect of host Chlorella NC64A carbon: phosphorus ratio on the production of Paramecium bursaria Chlorella Virus-1. *Freshwater Biology* **52,** 112–122 (2007).

17. Waldbauer, J. R., Coleman, M. L., Rizzo, A. I., Campbell, K. L., Lotus, J. & Zhang, L. Nitrogen sourcing during viral infection of marine cyanobacteria. *Proceedings of the National Academy of Sciences* **116,** 15590–15595 (2019).

18. Delbrück, M. The burst size distribution in the growth of bacterial viruses (bacteriophages). *Journal of Bacteriology* **50,** 131–135 (1945).

19. De Paepe, M., De Monte, S., Robert, L., Lindner, A. B. & Taddei, F. Emergence of variability in isogenic *Escherichia coli* populations infected by a filamentous virus. *PLoS One* **5,** e11823 (2010).

20. Kirzner, S., Barak, E. & Lindell, D. Variability in progeny production and virulence of cyanophages determined at the single-cell level. *Environmental Microbiology Reports* **8,** 605–613 (2016).

21. Dominguez-Mirazo, M., Harris, J. D., Demory, D. & Weitz, J. S. Accounting for cellular-level variation in lysis: implications for virus–host dynamics. *mBio* **15,** e01376–24 (2024).

22. Hinson, A., Papoulis, S., Fiet, L., Knight, M., Cho, P., Szeltner, B., Sgouralis, I. & Talmy, D. A model of algal-virus population dynamics reveals underlying controls on material transfer. *Limnology and Oceanography* **68,** 165–180 (2023).

23. Campos, D., Méndez, V. & Fedotov, S. The effects of distributed life cycles on the dynamics of viral infections. *Journal of Theoretical Biology* **254,** 430–438 (2008).

24. Wedd, C., Yunusov, T., Smith, A., Li, R., Hardo, G., Hunter, M., Majed, R., Fusco, D. & Bakshi, S. Single-cell imaging of the lytic phage life cycle dissects the timing and noise in individual infection steps. *bioRxiv,* 2024–04 (2024).

25. Dennehy, J. J. & Wang, I.-N. Factors influencing lysis time stochasticity in bacteriophage λ. *BMC Microbiology* **11,** 1–12 (2011).

26. Kannoly, S., Gao, T., Dey, S., Wang, N., Singh, A. & Dennehy, J. J. Optimum threshold minimizes noise in timing of intracellular events. *Iscience* **23** (2020).

27. Baker, C. W., Miller, C. R., Thaweethai, T., Yuan, J., Baker, M. H., Joyce, P. & Weinreich, D. M. Genetically determined variation in lysis time variance in the bacteriophage φX174. *G3: Genes, Genomes, Genetics* **6,** 939–955 (2016).

28. Stanier, R. & Cohen-Bazire, G. Phototrophic prokaryotes: the cyanobacteria. *Annual Review of Microbiology* **31,** 225–274 (1977).

29. Flombaum, P., Gallegos, J. L., Gordillo, R. A., Rincón, J., Zabala, L. L., Jiao, N., Karl, D. M., Li, W. K., Lomas, M. W., Veneziano, D., *et al.* Present and future global distributions of the marine cyanobacteria *Prochlorococcus* and *Synechococcus*. *Proceedings of the National Academy of Sciences* **110,** 9824–9829 (2013).

30. Avrani, S., Wurtzel, O., Sharon, I., Sorek, R. & Lindell, D. Genomic island variability facilitates Prochlorococcus–virus coexistence. *Nature* **474,** 604–608 (2011).

31. Avrani, S. & Lindell, D. Convergent evolution toward an improved growth rate and a reduced resistance range in Prochlorococcus strains resistant to phage. *Proceedings of the National Academy of Sciences* **112,** E2191–E2200 (2015).

32. Marston, M. F., Pierciey Jr, F. J., Shepard, A., Gearin, G., Qi, J., Yandava, C., Schuster, S. C., Henn, M. R. & Martiny, J. B. Rapid diversification of coevolving marine Synechococcus and a virus. *Proceedings of the National Academy of Sciences* **109,** 4544–4549 (2012).

33. Clokie, M. R., Kropinski, A. M. & Lavigne, R. *Bacteriophages, Methods and Protocols* (Springer, 2009).

34. Kannoly, S., Oken, G., Shadan, J., Musheyev, D., Singh, K., Singh, A. & Dennehy, J. J. Single-cell approach reveals intercellular heterogeneity in phage-producing capacities. *Microbiology Spectrum* **11,** e02663–21 (2023).

35. Russell, A. B., Trapnell, C. & Bloom, J. D. Extreme heterogeneity of influenza virus infection in single cells. *Elife* **7,** e32303 (2018).

36. Jones, J. E., Le Sage, V. & Lakdawala, S. S. Viral and host heterogeneity and their effects on the viral life cycle. *Nature Reviews Microbiology* **19,** 272–282 (2021).

37. Hevroni, G., Vincent, F., Ku, C., Sheyn, U. & Vardi, A. Daily turnover of active giant virus infection during algal blooms revealed by single-cell transcriptomics. *Science Advances* **9,** eadf7971 (2023).

38. Joffe, N., Kuhlisch, C., Schleyer, G., Ahlers, N. S., Shemi, A. & Vardi, A. Cell-to-cell heterogeneity drives host–virus coexistence in a bloom-forming alga. *The ISME Journal* **18,** wrae038 (2024).

39. Golding, I. Infection by bacteriophage lambda: an evolving paradigm for cellular individuality. *Current Opinion in Microbiology* **43,** 9–13 (2018).

40. Cahill, J. & Young, R. Phage lysis: multiple genes for multiple barriers. *Advances in Virus Research* **103,** 33–70 (2019).

41. Zheng, Y., Struck, D. K., Dankenbring, C. A. & Young, R. Evolutionary dominance of holin lysis systems derives from superior genetic malleability. *Microbiology* **154,** 1710–1718 (2008).

42. Amir, A., Kobiler, O., Rokney, A., Oppenheim, A. B. & Stavans, J. Noise in timing and precision of gene activities in a genetic cascade. *Molecular Systems Biology* **3,** 71 (2007).

43. Singh, A. & Dennehy, J. J. Stochastic holin expression can account for lysis time variation in the bacteriophage λ. *Journal of the Royal Society Interface* **11,** 20140140 (2014).

44. Ghusinga, K. R., Dennehy, J. J. & Singh, A. First-passage time approach to controlling noise in the timing of intracellular events. *Proceedings of the National Academy of Sciences* **114,** 693–698 (2017).

45. Mondal, A., Teimouri, H. & Kolomeisky, A. B. Molecular mechanisms of precise timing in cell lysis. *Biophysical Journal* **123,** 3090–3099 (2024).

46. You, L., Suthers, P. F. & Yin, J. Effects of *Escherichia coli* physiology on growth of phage T7 in vivo and in silico. *Journal of Bacteriology* **184,** 1888–1894 (2002).

47. Storms, Z. J., Brown, T., Cooper, D. G., Sauvageau, D. & Leask, R. L. Impact of the cell life-cycle on bacteriophage T4 infection. *FEMS Microbiology Letters* **353,** 63–68 (2014).

48. Hadas, H., Einav, M., Fishov, I. & Zaritsky, A. Bacteriophage T4 development depends on the physiology of its host *Escherichia coli*. *Microbiology* **143,** 179–185 (1997).

49. Wang, I.-N. Lysis timing and bacteriophage fitness. *Genetics* **172,** 17–26 (2006).

50. Abedon, S. T. Selection for bacteriophage latent period length by bacterial density: a theoretical examination. *Microbial Ecology* **18,** 79–88 (1989).

51. Wang, I.-N., Dykhuizen, D. E. & Slobodkin, L. B. The evolution of phage lysis timing. *Evolutionary Ecology* **10,** 545–558 (1996).

52. Abedon, S. T., Herschler, T. D. & Stopar, D. Bacteriophage latent-period evolution as a response to resource availability. *Applied and Environmental Microbiology* **67,** 4233–4241 (2001).

53. Bull, J., Pfennig, D. W. & Wang, N. Genetic details, optimization and phage life histories. *Trends in Ecology & Evolution* **19,** 76–82 (2004).

54. Bull, J. Optimality models of phage life history and parallels in disease evolution. *Journal of Theoretical Biology* **241,** 928–938 (2006).

55. Heineman, R. H. & Bull, J. J. Testing optimality with experimental evolution: lysis time in a bacteriophage. *Evolution* **61,** 1695–1709 (2007).

56. Abedon, S. T. in *Evolutionary Biology: Contemporary and Historical Reflections Upon Core Theory* 375–426 (Springer, 2023).

57. Clokie, M. R. & Mann, N. H. Marine cyanophages and light. *Environmental Microbiology* **8,** 2074–2082 (2006).

58. Liu, R., Liu, Y., Chen, Y., Zhan, Y. & Zeng, Q. Cyanobacterial viruses exhibit diurnal rhythms during infection. *Proceedings of the National Academy of Sciences* **116,** 14077–14082 (2019).

59. Puxty, R. J., Evans, D. J., Millard, A. D. & Scanlan, D. J. Energy limitation of cyanophage development: implications for marine carbon cycling. *The ISME journal* **12,** 1273–1286 (2018).

60. Wyman, M., Gregory, R. & Carr, N. Novel role for phycoerythrin in a marine cyanobacterium, *Synechococcus* strain DC2. *Science* **230,** 818–820 (1985).

61. Lindell, D., Padan, E. & Post, A. F. Regulation of ntcA expression and nitrite uptake in the marine *Synechococcus* sp. strain WH 7803. *Journal of Bacteriology* **180,** 1878–1886 (1998).

62. Brahamsha, B. A genetic manipulation system for oceanic cyanobacteria of the genus *Synechococcus*. *Applied and Environmental Microbiology* **62,** 1747–1751 (1996).

63. Lindell, D. The Genus *Prochlorococcus*, Phylum Cyanobacteria (2014).

64. Moore, L. R., Coe, A., Zinser, E. R., Saito, M. A., Sullivan, M. B., Lindell, D., Frois-Moniz, K., Waterbury, J. & Chisholm, S. W. Culturing the marine cyanobacterium *Prochlorococcus*. *Limnology and Oceanography: Methods* **5,** 353–362 (2007).

65. Morris, J. J., Kirkegaard, R., Szul, M. J., Johnson, Z. I. & Zinser, E. R. Facilitation of robust growth of *Prochlorococcus* colonies and dilute liquid cultures by "helper" heterotrophic bacteria. *Applied and Environmental Microbiology* **74,** 4530–4534 (2008).

66. Ge, H., Xu, K. & Ghahramani, Z. *Turing: a language for flexible probabilistic inference* in *International conference on artificial intelligence and statistics* (2018), 1682–1690.

67. Bezanson, J., Edelman, A., Karpinski, S. & Shah, V. B. Julia: A fresh approach to numerical computing. *SIAM Review* **59,** 65–98 (2017).

68. Inc., T. M. *MATLAB version: 24.1.0 (R2024a)* Natick, Massachusetts, United States, 2024. https://www.mathworks.com.

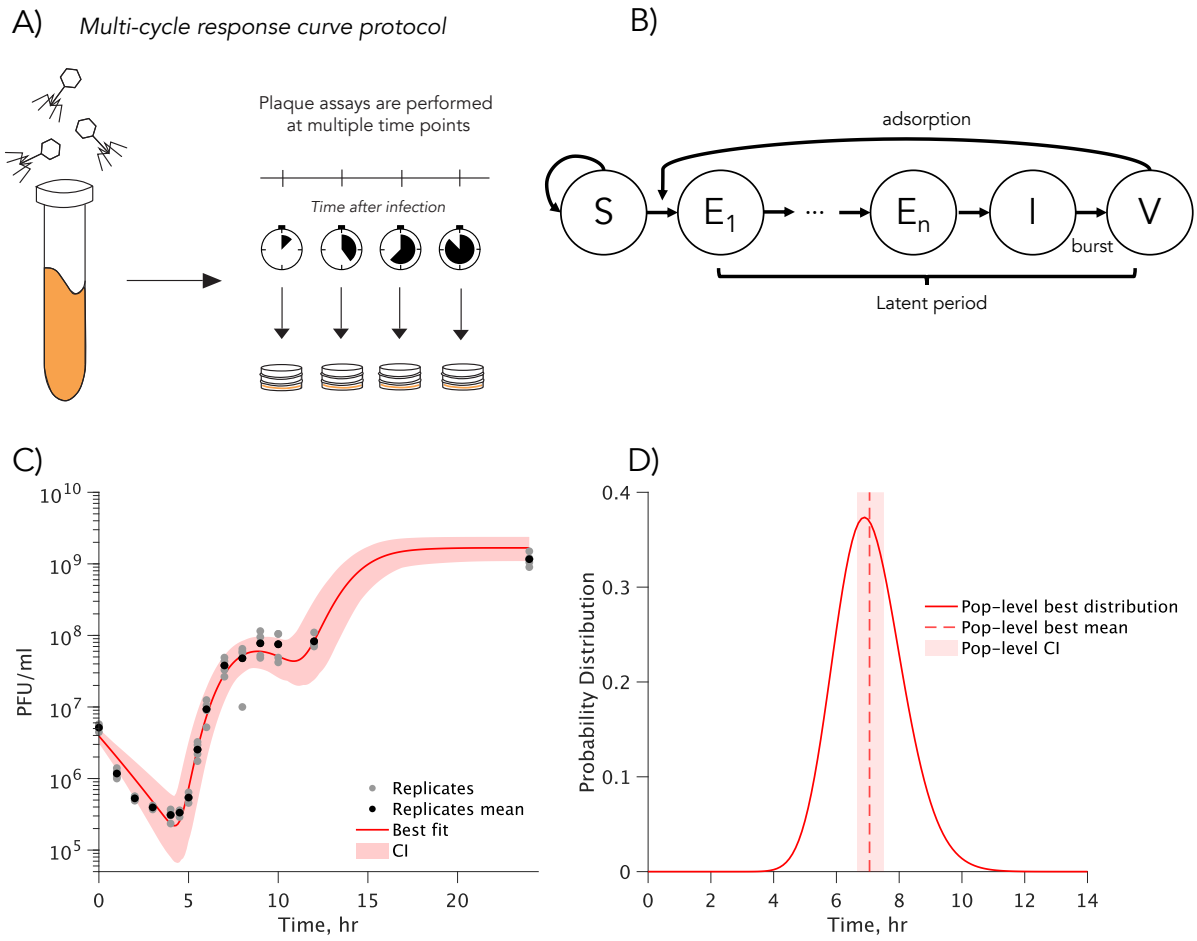

Figure 1: **Predicting single-cell heterogeneity from population-level data.** We model lysis time heterogeneity in a *Synechococcus* population infected by cyanophage Syn9 using viral density time-series data. **A)** A 'multi-cycle response curve' is generated by infecting the cyanobacterial population with the cyanophage. Samples are collected at multiple time points, and viral density is quantified via plaque assays. **B)** In this compartmental model of lytic viral infection, infectious viral particles (V) adsorb to susceptible cells (S). Infected cells progress through several intermediate stages of infection (E_1 to E_n) before reaching the actively infected state (I). Infected cells lyse, releasing new viral particles. The mean time for a cell to transition from the first intermediate infection stage (E_1) to final lysis is the mean latent period. The number of intermediate infection stages (n) modulates the coefficient of variation (CV) of the latent period distribution. **C)** Using data from four experimental replicates, we determine the parameters that best fit the lysis infection model to the observed viral dynamics from the multi-cycle response curve. Shaded regions represent a 95% confidence interval (CI). **D)** Among the predicted parameters, we estimate the latent period distribution of the population. The mean latent period is predicted to be 7 hr [CI: 6.7, 7.5], and the CV is 0.15 [CI: 0.13, 0.18].

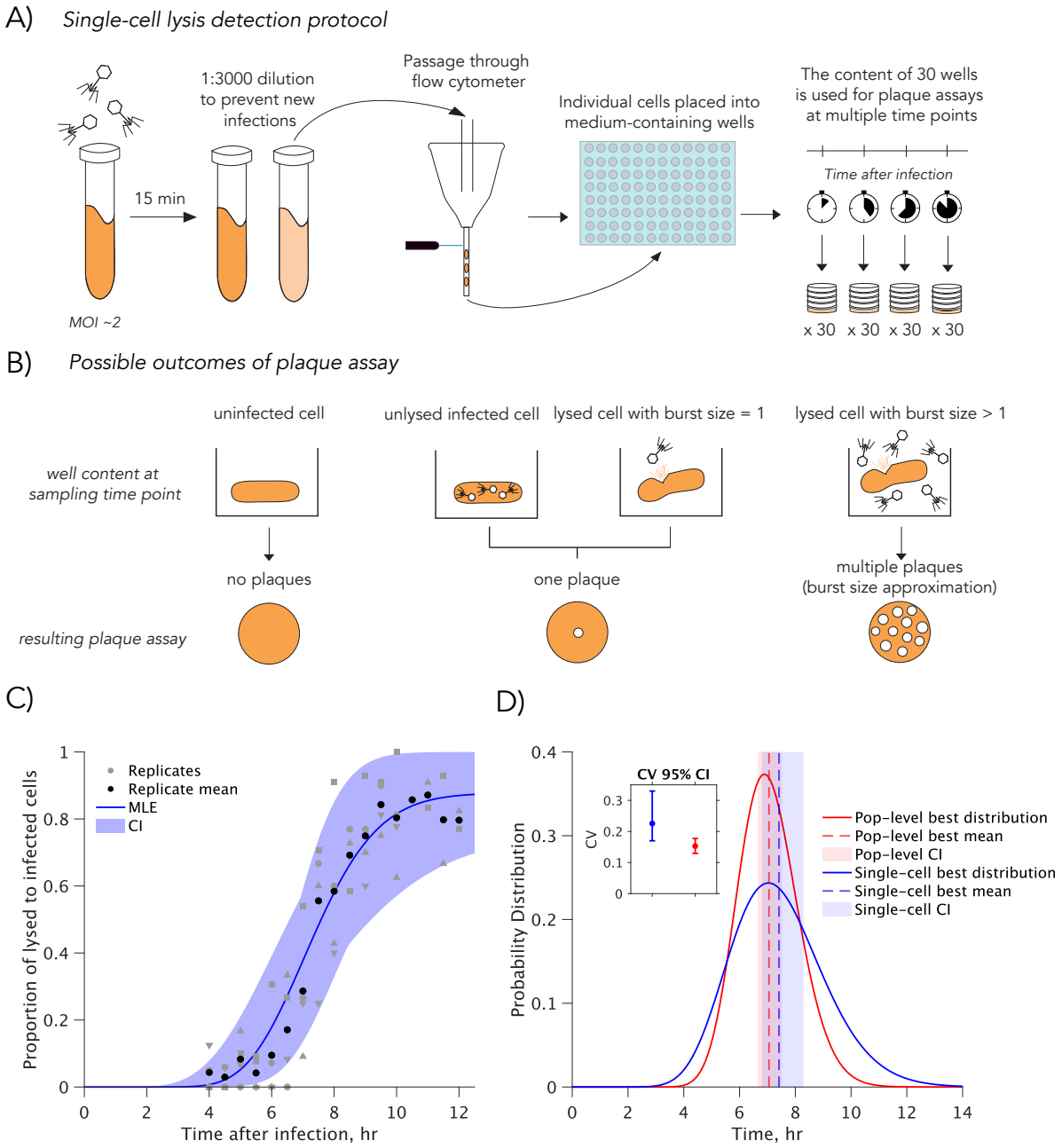

Figure 2: **Single-cell heterogeneity in lysis time. A)** A 'single-cell lysis detection protocol' was developed to reconstruct the Cumulative Distribution Function (CDF) of a virus-microbe latent period. A microbial population is inoculated with phage, and after 15 minutes, the population is diluted to prevent further infections. The population is then passed through a flow cytometer, where individual cells are isolated and placed into wells. At multiple time points, the contents of 30 wells are harvested for plaque assays to assess infection status. **B)** At each time point, plaque assays can yield three outcomes: i) no plaques for uninfected cells, ii) a single plaque for cells that were infected but not yet lysed, or for lysed cells with a burst size of 1, and iii) multiple plaques for cells that lysed and released multiple infective viruses. The number of assays with one or more plaques reflects the number of infected cells. Assuming few infections with a burst size of one, the proportion of lysed cells is approximated by the ratio of assays with multiple plaques to the total number of infected cells. **C)** Prediction of the latent period CDF based on 4 experimental replicates of the 'single-cell lysis detection' method (gray symbols). The solid line indicates the best fit, while the shaded region represents the 95% CI. The different-shaped gray symbols indicate the different biological replicates. **D)** The Probability Distribution Function (PDF) of the latent period derived from population-level viral density time series (Figure 1, red) and the Cumulative Distribution Function (CDF) from the single-cell lysis detection method (blue). The CI for both the mean latent period (shaded region) and the coefficient of variation (CV, figure inset) overlap.

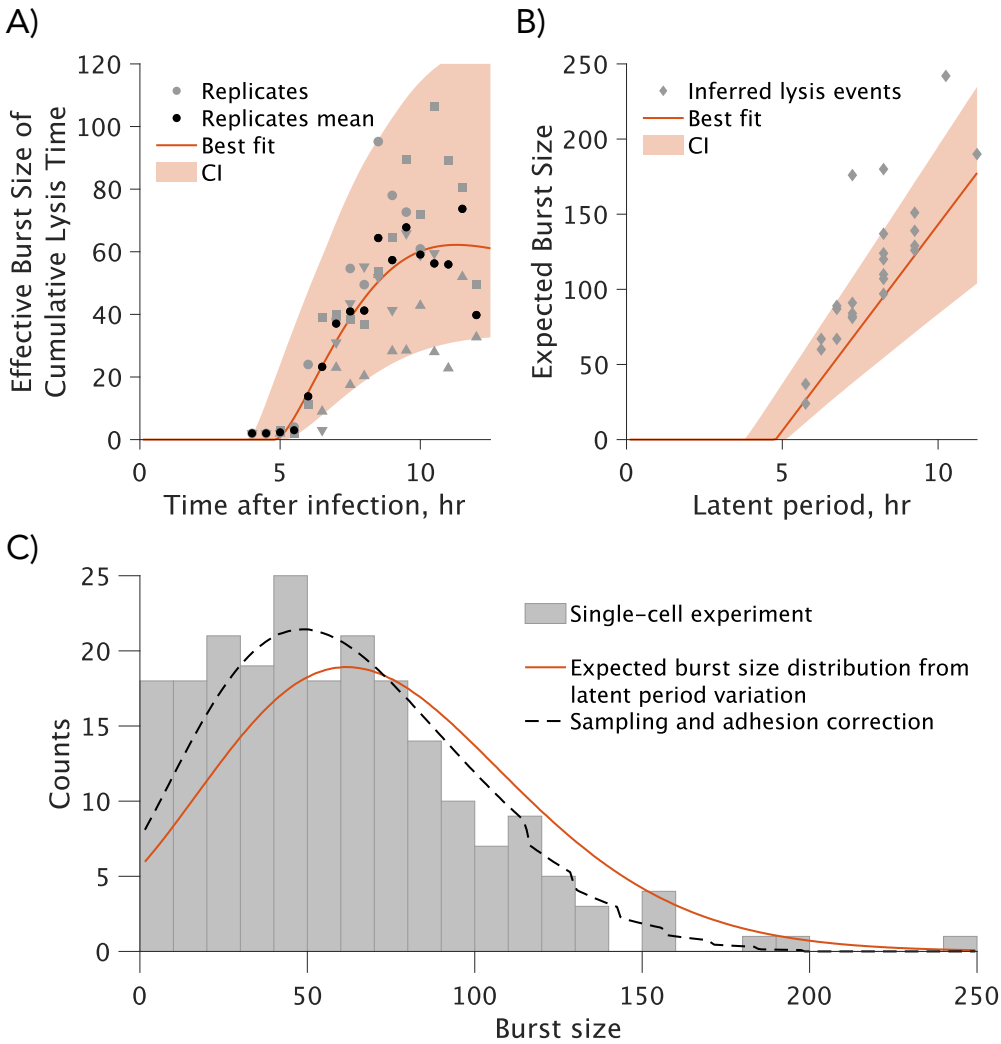

Figure 3: **Relationship between burst size and latent period. A)** The average burst size at each sample time point from the 'single-cell lysis detection method' reflects the interplay between the latent period distribution and the burst size-latent period relationship. This relationship is inferred using the previously predicted latent period distribution. The different-shaped gray symbols indicate the different biological replicates. **B)** The predicted relationship shows a linear increase in burst size as a function of latent period, with a rate of progeny production of 27.4 viral particles per hour [CI: 15.0, 34.9], beginning at 4.8 hr [CI: 3.7, 5.2] post-infection. The burst sizes from inferred lysis events (gray diamonds, see Methods) support this linear relationship. **C)** The burst size distribution using all plaque assays starting at 9 hr after infection (n = 213, gray bars) is compared to the expected burst size distribution derived from our predictions of latent period PDF and latent period to burst size relationship (solid orange line), and to the distribution we expect to observe when we correct for sampling at different timepoints, and for time-dependent viral particle adhesion to well surfaces (dashed line).